Coupled convective pendulums

Peter Frick, Andrei Sukhanovskii,* and Andrei Vasiliev

Institute of Continuous Media Mechanics,

Academ. Korolyov, 1, Perm, 614013, Russia

Sergey Filimonov and Andrei Gavrilov

Kutateladze Institute of Thermophysics SB RAS,

Lavrentieva av. 1, Novosibirsk, 630090, Russia

(Dated: December 8, 2025)

Abstract

An extended body, free floating nearby one of horizontal boundaries in a convective cell heated from below and cooled from above, with a suitable set of control parameters, provides the convective pendulum mode in which the body performs regular oscillatory movements from one side wall to the other. In this paper, we considered numerically in the simplest two-dimensional formulation a convective cell at moderate Rayleigh numbers ($\mathrm{Ra} \approx 5 \times 10^5 - 5 \times 10^6$) with two bodies (plates) floating at different depths. Two convective pendulums in one cell are subject to a complex mutual influence determined by the geometry of the cavity, the size and the depth of immersion of the plates and the intensity of heating, leading to a wide variety of observed modes. The dynamics of large plates (of the order of half the horizontal size of the cell or more) strongly depend on the depth of immersion and include convective pendulum mode with regular antiphase oscillations, irregular fluctuations, full stops and synchronized periodic movements. The dynamics of two plates of relatively small size is fundamentally different and unexpected. The complex interaction between the small plates leads to the modes with a pronounced intermittent character, when intervals of quasi-periodic movements of both plates are replaced by low-amplitude oscillations against the background of random wandering throughout the cell. During full-amplitude oscillations, the plates move quasi-periodically but with a random phase shift. The very specific behavior was observed during random walks, in which the plates perform small-scale chaotic oscillations, without breaking away from each other, as if they are on a flexible bundle.

I. INTRODUCTION

The dynamics and structure of convective flows in closed volumes are very diverse and depend significantly on the geometry of the cavity, the heating intensity (Rayleigh number), the properties of the fluid (Prandtl number), and boundary conditions [1–3]. A new and rather wide range of problems emerges when considering convective systems with free-floating extended bodies, which are entrained by the convective flow and, in turn, influence heat and mass transfer within the fluid. The first problems of this type were considered in experimental studies in which a solid body had one horizontal degree of freedom [4, 5].

* san@icmm.ru

Two different cases were studied: one with a heat-insulating object floating on a free surface [4] and the other with an immersed body that freely floats in the horizontal direction at a specific depth [5]. The problem of a body on the free surface has been actively studied in a number of experimental and numerical investigations in the context of the movement of tectonic plates by convective flows in the Earth's mantle [6, 7], and continues to attract great attention as a complex dynamic system [8, 9]. Along with various geophysical applications, the problem of a immersed body can also be interesting from a fundamental point of view. It leads to a wide variety of dynamic modes, both for one-dimensional body movements [10, 11] and for two-dimensional body wanderings in an extended horizontal layer [12, 13].

An obvious generalisation of the problem of convection in a cavity with a free-floating object is the problem of convection with multiple floating objects (two, three or more), which can arise in various technological and natural settings. There are several studies that have examined the movement of bodies under the influence of convection flows. The self-organization of large numbers of small spherical bodies has been demonstrated in [14], and the motion of polygonal plates, which mimic tectonic plates, has been explored in [15].

The studies of convective flows with a single floating body were motivated as well by a fundamental interest in dynamic systems of convective nature that demonstrate various mechanisms of chaotic behavior and organization. It was found that an immersed insulating plate floating in the vicinity of the horizontal thermal boundary layers (or along a free surface) demonstrates stable oscillatory movements (regime of a "convective pendulum"). This regime loses stability as the body moves further away from the boundary and/or as the Rayleigh number increases [4, 5]. Obviously, the introduction of a second free-floating body into the system (for example, floating near another horizontal boundary) can significantly complicate the dynamics of the system. One can expect the emergence of "coupled convective pendulums" with complex dynamics due to the non-linearity of the interactions between the various components of the system under consideration. This problem is addressed in this paper using numerical modeling in its simplest two-dimensional form.

Specifically, we consider a horizontally elongated rectangular cavity filled with an incompressible liquid, in which two plates float freely in the horizontal direction, at various (but fixed) depths. The influence of the plate size (the sizes of both plates are considered the same), the depth of immersion of each plate, and the intensity of heating on the plate movement characteristics is studied. It is shown that regimes with synchronized motion of

the plates are indeed possible. Moreover, plate oscillations can occur in both phase and antiphase, and synchronization mechanisms can be either global or local in nature. A complex dynamic was observed in a convective system with two relatively small plates floating near opposite heat exchangers. It turned out that they feel each other quite well, demonstrating independent random fluctuations on short time-space scales, but tracking each other's behavior on large time-space scales.

The paper is organized as follows. The statement of the problem, description of numerical model and governing parameters are given in section II. The main results are presented in section III and include the description of dynamic modes for the large plates (subsection III A), the influence of Rayleigh number (subsection III B), the dynamics of small plates (subsection III C) and the behavior of integral characteristics (subsection III D). A summary and conclusions are given in section IV.

II. METHODS

A mathematical model of free-convective fluid flow with a moving submerged solid body was implemented and verified in [16]. The model was used for simulations in both two-dimensional [10] and three-dimensional formulations [11, 17], but only in case of a single submerged body. In this paper, we developed the numerical model for the case of multiple non-interacting submerged solid bodies and considered the problem of a natural convection in a cavity with two horizontally floating plates. We consider a rectangular cell filled with water, in which two thin plates are submerged at different depths (Fig. 1). The parameters associated with the top and bottom plates are denoted by index 1 and index 2, respectively. The plates have one degree of freedom and can only move horizontally along the long side of the cavity perpendicular to the direction of gravity.

Numerical model includes the equations of free convection of an incompressible fluid in the Oberbeck-Boussinesq approximation, and the equations of motion and heat transfer for the immersed movable solid plates. The unsteady fluid flow is described by the Navier-Stokes equations, which includes the buoyancy force, and the heat transfer equation in the

dimensional form

$$\nabla \cdot \mathbf{u} = 0,$$
$$\frac{\partial \mathbf{u}}{\partial t} + (\mathbf{u} \cdot \nabla)\,\mathbf{u} = -\frac{\nabla p}{\rho} + \nu \nabla^2 \mathbf{u} - \mathbf{g}\beta(T - T_0),$$
$$\rho C_p \left(\frac{\partial T}{\partial t} + (\mathbf{u} \cdot \nabla)\,T \right) = \nabla \cdot (\lambda \nabla T)\,,$$

where $\mathbf{u}$ is the velocity, ρ is the density, T is the temperature, T_0 is the reference temperature, p is the pressure, $\mathbf{g}$ is the acceleration due to gravity (directed in the opposite direction of the axis z), C_p is the heat capacity, ν is the kinematic viscosity, β is the thermal expansion coefficient, and λ is the heat conductivity coefficient.

For each plate the equation of motion is solved separately. Newton's equation describes the motion of the solid plate,

$$\frac{d\mathbf{V}}{dt} = \frac{\mathbf{f}}{m},$$

where $\mathbf{V}$ is the vector of plate velocity, $\mathbf{f}$ is the force acting from the liquid on the solid body, m is the mass of the plate. The plate velocity is purely horizontal, the vertical component of the velocity is artificially set to zero $V_z = 0$. The net forces are calculated by integrating over the entire surface of the specific plate (horizontal and vertical faces),

$$\mathbf{f} = \oint_{\Gamma_b} (p\mathbf{n} - \tau_{\mathbf{w}})\, dS,$$

where $\tau_{\mathbf{w}}$ is the viscous stress on the wall, $\mathbf{n}$ is the unit vector normal to the surface, and dS is the surface element, Γ_b describes the plate surface. The impact of the plate into the wall is considered inelastic. The model of the solid plate motion in the fluid is implemented using the Immersed Boundary Method [18]. A detailed description of the mathematical model and results of its testing are presented in [16].

No-slip boundary conditions are imposed on the fluid velocity at all solid boundaries:

$$\mathbf{u} = 0.$$

The side walls of the cavity are assumed to be adiabatic, and fixed temperature at top and bottom cavity boundaries is set:

$$\left.\frac{\partial T}{\partial n}\right|_{sidewall} = 0, \qquad T|_{z=0} = T_h, \qquad T|_{z=H} = T_c.$$

The physical properties of water are specified for normal conditions ($\rho = 998.15$ kg/m^3, $\nu = 10^{-6}$ m^2/s, $\lambda = 0.598$ W/(m·K), $C_p = 4183$ J/(kg·K), $\beta = 0.000211$ 1/K). The physical

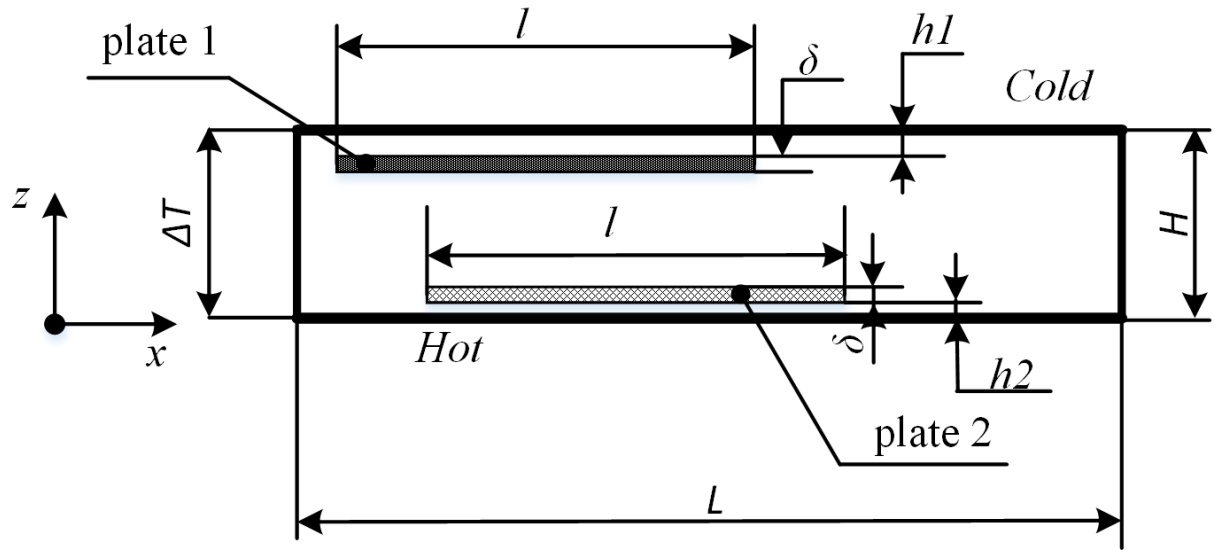

FIG. 1. Schematic of the problem.

properties of the plates are identical: the density $\rho_p = 1300\ kg/m^3$ and the thermal capacity $\lambda_p = 0.38\ J/(mK)$. The geometry of the cavity are fixed in all calculations $L = 90\,\text{mm}$, $H = 20\,\text{mm}$ (aspect ratio $\Gamma = L/H = 4.5$), plate thickness $\delta = 1\,\text{mm}$. The vertical position of the plates is characterized by a dimensionless distance d. For the top plate, this parameter is $d1 = h1/H$, where $h1$ is the distance from the top wall of the cavity to the upper edge of the plate. In the cases considered $d1 = 0.1$. For the bottom plate $d2 = h2/H$, where $h2$ is the distance from the bottom of the cavity to the lower edge of the plate. Seven different values of $d2$ were considered, ranging from 0.1 to 0.7. These cases will be denoted as d1d1, d1d2, ..., d1d6, and d1d7, respectively. The horizontal size l of both plates is the same and is varied within the range $L/8 \le l \le 3L/4$.

Numerical simulations were performed with the in-house CFD (Computational Fluid Dynamics) code *σFlow*, whose numerical algorithm is based on the finite volume method for the unstructured spatial grid. The approximation of the convective and diffusion terms in the Navier-Stokes equation is carried out by the second-order central-difference schemes. The coupling between the velocity and pressure fields, which ensures the continuity equation, is realized using a SIMPLE-like (Semi-Implicit Method for Pressure-Linked Equations) splitting procedure [19]. The values of the velocity and pressure fields are determined at the centers of the control volumes. To eliminate oscillations of the pressure field, the Rhie-Chow approach is used, which consists of a special interpolation of the velocity vector on the faces

of the control volumes [20]. The second order Crank-Nicolson method is used for the time integration of the equation of motion. Both the viscous and the convective terms of the equation of motion are treated implicitly. The convective terms of the energy transfer equation are approximated by a second order upwind TVD (Total Variation Diminishing) scheme [21], and the unsteady term of the temperature equation is approximated by a second order three-layer scheme.

Thermal convection is governed by the following nondimensional parameters: the Rayleigh number Ra, which is the ratio of buoyancy to dissipative forces, and the Prandtl number Pr which is the ratio of kinematic viscosity ν to thermal diffusivity χ

$$\mathrm{Ra} = \frac{g\beta\Delta T H^3}{\nu\chi}, \qquad \mathrm{Pr} = \frac{\nu}{\chi},$$

where $\Delta T = T_h - T_c$ is the temperature drop between the lower and upper boundary.

Numerical simulations were performed for two values of Rayleigh number $\mathrm{Ra} = 3.7 \times 10^5$ and $\mathrm{Ra} = 3.7 \times 10^6$ for the fixed Prandtl number $\mathrm{Pr} = 6.6$.

The dimensionless Nusselt number Nu and Reynolds number Re characterize the global heat and momentum transfer. Within Oberbeck-Boussinesq approximation, the Nusselt number is

$$\mathrm{Nu} = \frac{H}{\Delta T} \langle \frac{\partial T}{\partial z}\Big|_{z=0} \rangle_{x,t}$$

where $\langle\cdot\rangle_{x,t}$ denotes averaging over time and over horizontal coordinate x and $z = 0$ corresponds to the bottom.

For the Reynolds number we use the definition, which is based on the mean square root of the fluid velocity

$$\mathrm{Re} = \frac{H\sqrt{\langle \mathbf{u}\cdot\mathbf{u}\rangle_{t,V}}}{\nu},$$

where $\langle\cdot\rangle_{t,V}$ denotes averaging over time and over the entire convection cell.

III. RESULTS

A. Two relatively large plates immersed at different depths

We start by considering two plates whose length is equal to half the length of the cavity $l = L/2$, immersed at different depth. We chose this size because a system with a single

plate of this size was studied in detail earlier for a wide range of Rayleigh numbers and plate immersion depths [10]. All simulations described in this subsection are realized for a fixed Rayleigh number $\mathrm{Ra} = 3.7 \times 10^5$.

The character of movement of the plates of this size at different positions of the lower plate (the upper plate in all simulations was immersed at depth $d1 = 0.1$) is illustrated in left column of Fig. 2, which shows the movements of the centers of both plates during each numerical experiment lasting 5000 seconds ($x = 0$ corresponds to the center of the cell).

It is known that one plate of this size, located in a layer of the same geometry at a distance of $d1 = 0.1$ from one of the horizontal heat exchangers, performs at such Rayleigh number regular oscillatory movements from one side wall to the other, realizing the convective pendulum mode [10]. In the system with two plates, a pair of connected pendulums appears, and the nature of this connection changes with the position of the second plate. If the plates are close to the opposite heat exchangers (case d1d1, Fig. 2(left)), then they move in antiphase. This type of movement is caused by the formation of a large vortex between the plates, which pulls them in opposite directions (see the schematic drawing in Fig. 3(a,b)).

If the lower plate rises up from the bottom, the regularity of the movements of both plates is disrupted. In case d1d3, after some oscillations both plates stop (Fig. 2(left)). When the gap between the plates decreases further they resume their movement. While the lower plate floats near the central plane (cases d1d4 and d1d5), the movements are rather chaotic, but as the lower plate approaches the upper boundary (cases d1d6 and d1d7) the movements become completely regular. Moreover, the movements of both plates become synchronized (see Fig. 2(left)). At this position of the plates, the main vortex forms between the bottom and the lower plate, determining the movements of the lower plate (Fig. 3(c,d)), and the upper plate follows the lower one. The mechanism of case d1d6, in which the plates move almost synchronously, is not obvious. In this case, when the lower plate is detached, by the action of convective vortex from the side wall, it opens access to the convective flow to the upper plate. Than a stream rushes into the gap between the plates, which drags the upper plate behind the lower one (Fig. 3(c)). After the upper plate is detached, both plates rush to the opposite wall, with the lower one always leading. When the lower plate approaches the opposite wall, it blocks the flow between the plates, which leads to its suppression and deceleration of the upper plate (Fig. 3(d)). The effect becomes more pronounced if

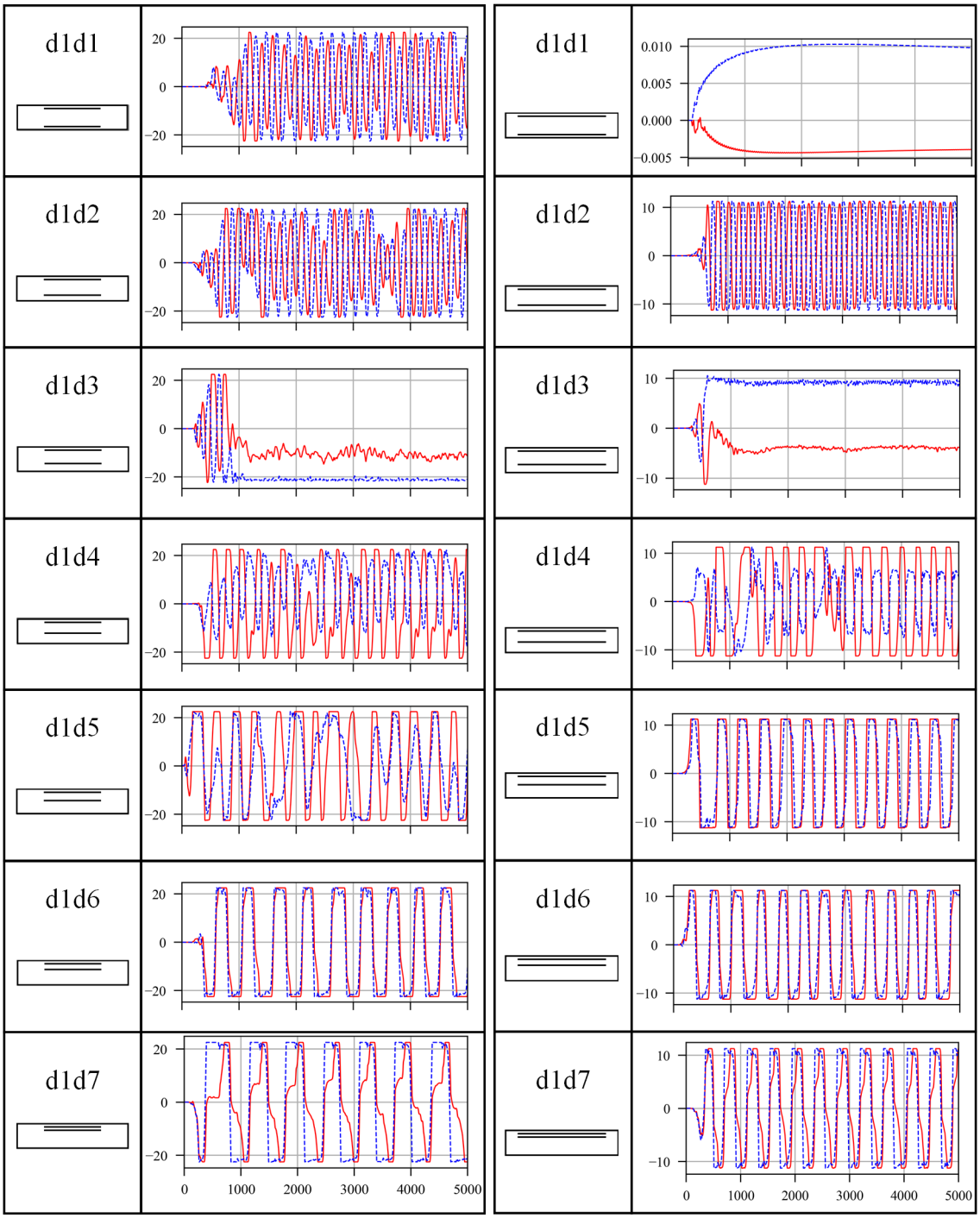

FIG. 2. The movement of the centers of the plates of size $l = L/2$ (left) and $l = 3L/4$ (right) at $\mathrm{Ra} = 3.7 \times 10^5$ for different cases, marked in each panel. The position of the lower plate is shown by blue dotted line, the position of the upper plate – by red solid line.

we reduce the gap between plates (case d1d7). In this case the flow between two plates becomes weaker and it takes more time for the upper plate to rush after the lower one. As

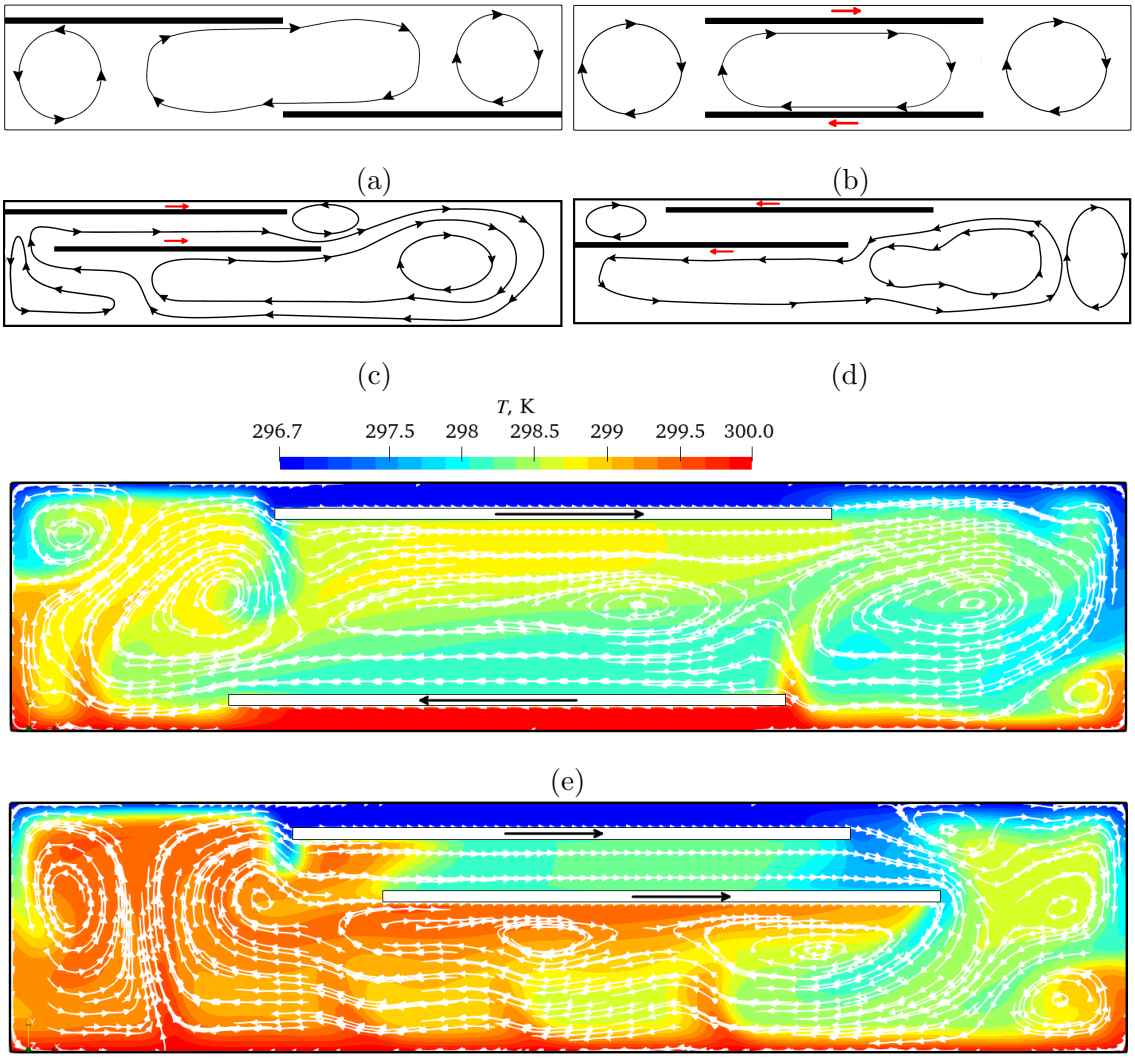

FIG. 3. The structure of the convective flow in the cell with two plates of size $l = L/2$ at $\mathrm{Ra} = 3.7 \times 10^5$. Schematic representation of the main flow at different stages of the plate motion: (a) case d1d1, start of the plate motion from the opposite walls; (b) case d1d1, the plates move across the center; (c) case d1d6, the lower plate detaches from the wall; (d) case d1d6, the lower plate reaches the wall. Instantaneous temperature field and streamlines for two cases: d1d1 (e) and d1d6 (f) (the black arrows show the direction of motion of each plate).

a result the distance between the plate centers has become larger and the braking of the upper plate becomes more pronounced when the lower plate reaches the wall. Interestingly, after a sudden deceleration, the upper plate accelerates again and reaches the wall with a short delay relative to the lower plate. This is because the lower plate has been slightly

pushed away from the wall, creating a gap through which a stream of fluid rushes. Please note that the schematic drawings (Fig. 3) were created after averaging over specific stages of plate motion, in order to remove chaotic small-scale flows. The instantaneous temperature and velocity distributions are highly non-uniform. (Fig. 3(e,f)).

Second, we consider two larger plates ($l = 3L/4$), for which the available space to move is three times smaller than their own size. The set of illustration of the dynamics of both plates is presented in the right column of Fig. 2. In general, the character of plates dynamics remains similar in all cases except case d1d1 (compare the left and right columns in Fig. 2). In case d1d1 the both plates, after a short transient movement, stop near the center of the cell. It is curious that the convective flow at the same time demonstrates a pronounced oscillatory regime associated with the oscillations of the coupled side vortices (Fig. 4), which alternately reach the maximum and minimum of intensity in the upper and lower corners. The convective pendulum mode is observed when the lower plate is slightly shifted from the bottom (case d1d2). We can assume that the realization of this mode requires some asymmetry. If the bottom plate is located higher (case d1d3), then both plates also stop, but their position is not symmetrical, and no plate is adjacent to the side wall. The structure of the flow and temperature field when both plates are in rest is illustrated in Fig. 5. If the lower plate approach the upper one (cases d1d5, d1d6 and d1d7) both large plates ($l = 3L/4$) are involved in regular synchronous oscillations, similar to those described above for the plates of size $l = L/2$.

B. The plate motion at higher Rayleigh number

An increase in the Rayleigh number results in a more intense convective flow, which in turn leads to more intense and less organized plate motions. To illustrate the main trends related to the increase in the Rayleigh number, we performed a series of simulations for plates of the base size $l = L/2$, but for the Rayleigh number increased by an order of magnitude, that is, $\mathrm{Ra} = 3.7 \times 10^6$.

The oscillograms of the positions of the centers of the two plates for different immersion depth of the second plate (the immersion depth of the upper plate is fixed in all simulations, $d1 = 0.1$) are shown in Fig. 6. Comparison of this figure with Fig. 2(left column) shows that the dependence of the plates dynamics on the position of the second plate is generally

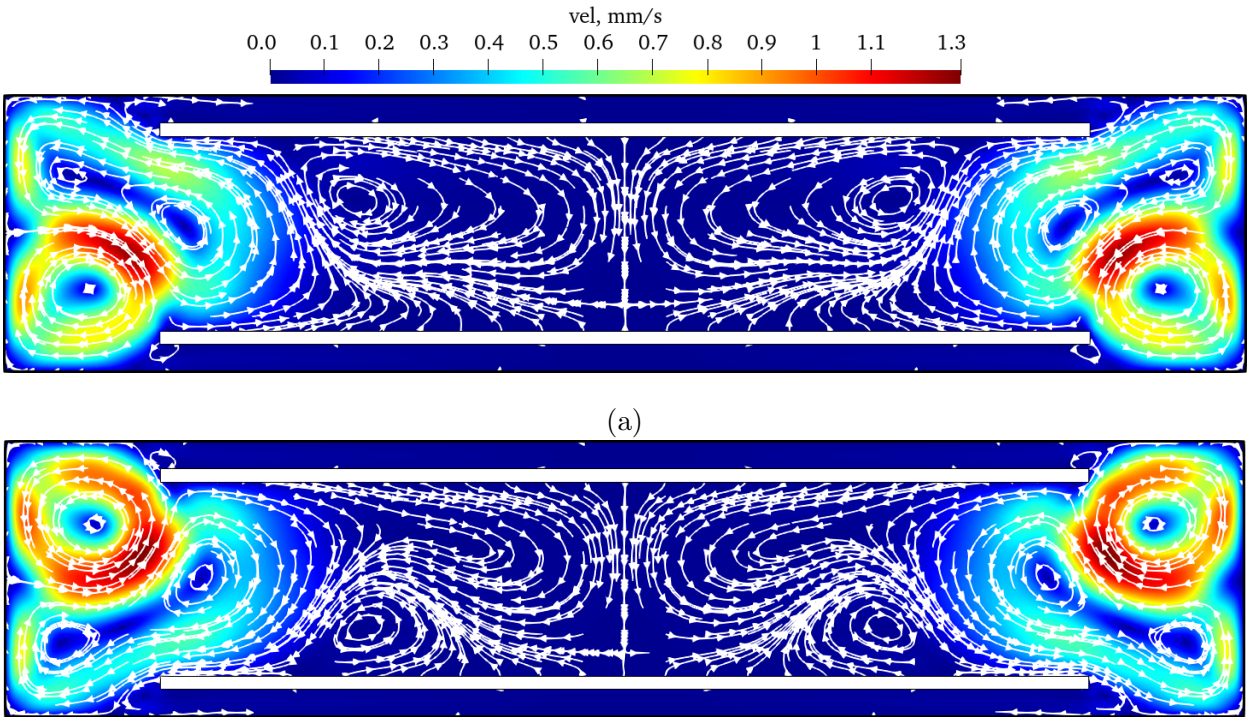

FIG. 4. Oscillatory mode of convective flow with standing plates of size $l = 3L/4$, case d1d1. (a) Corner vortices are above, (b) corner vortices are below. The time interval between two snapshots is ≈21s.

similar. If the plates are located near the opposite horizontal boundaries (case d1d1), they exhibit stable regular oscillations from one side wall to the other. The plates movements are still approximately anti-correlated, and their typical velocity increased significantly. At

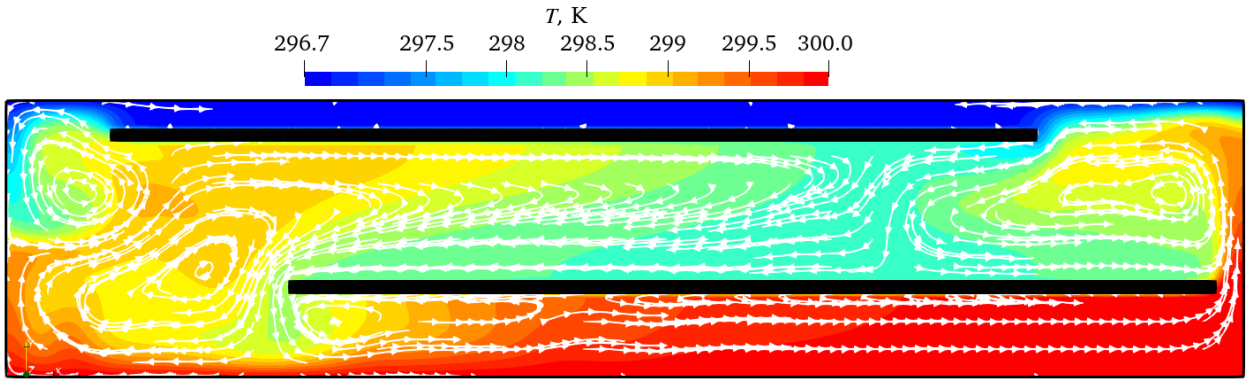

FIG. 5. The instantaneous temperature field with streamlines when the plates are in rest. Case d1d3, plates size $l = 3L/4$.

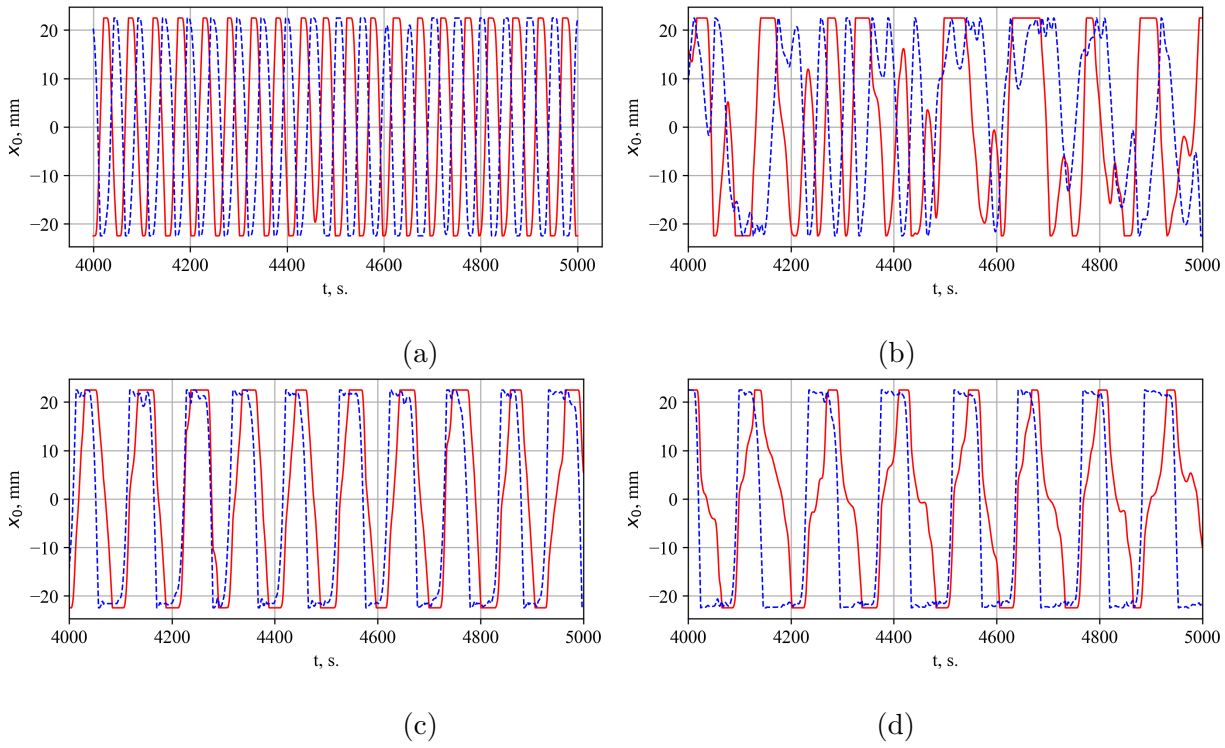

FIG. 6. The movement of the centers of the plates of size $l = L/2$ (lower plate – dotted line, upper plate – solid line) at $\mathrm{Ra} = 3.7 \times 10^6$ for different cases: d1d1 (a), d1d4 (b), d1d6 (c) and d1d7 (d).

$\mathrm{Ra} = 3.7 \times 10^5$, the average full cycle period was 187 seconds, and at $\mathrm{Ra} = 3.7 \times 10^6$ it decreased to 49.8 seconds (the ratio is 3.8, so the dependence of the velocity on the Rayleigh number exceeds the root square).

We showed in previous subsection that the dynamics of the plates changes fundamentally with the location of the lower plate. In particular, at $\mathrm{Ra} = 3.7 \times 10^5$ when the lower plate is located near the middle of the layer, after a transient process the upper plate presses against the side wall and the movement of both plates stopped. At $\mathrm{Ra} = 3.7 \times 10^6$, intense turbulent convective vortices prevent the plate from pressing against the wall, and both plates undergo chaotic, weakly coupled oscillations (see Fig. 6b).

In cases where both plates float in the upper part of the layer, the intensity of movements also increases, but the nature of the movements does not change (compare cases d1d6 and d1d7 in Fig. 2 and Fig. 6). In case d1d6 the period of the full cycle of plate movement decreased from 436 s to 98 s (the average frequency increased 4.5 times, that is, more than in case d1d1). In case d1d7 the average period dropped from 562 s to 123 s (the frequency increased 4.7 times), and the shape of the curve became less stable within one

cycle, especially for the upper plate.

C. Two relatively small plates immersed at different depths

Now, we are going to decrease the size of the plates, studying the behavior of a couple of plates of relatively small size. It is natural to expect that as the size of the plates decreases, their movements would become more independent and characterized by random uncorrelated walks at $l << L$. However, more complicate dynamics has been observed. To clarify this issue we return to the Rayleigh number $\mathrm{Ra} = 3.7 \times 10^5$ and study the motion of plates of size $l = L/4$ and $l = L/8$ (as before, both plates have the same size in each numerical experiment).

Results of simulations for the plates of size $l = L/4$ for different position of lower plate are shown in Fig. 7. The behavior of the plates $l = L/4$ in case d1d1 turned out to be the most interesting. Fig. 7(upper panel) gives the impression that the movements of both plates are correlated, which is inconsistent with the low value of the correlation coefficient. The plate motion in this case has a pronounced intermittent character - intervals of quasi-stable periodic movements are replaced by low-amplitude oscillations against the background of random wandering throughout the cell. Closer look shows that fragments with full-scale oscillations (from one side wall to another) demonstrate oscillations of both plates with a similar frequency, but with different (random) phase shifts. This explains low value of correlation coefficient. In contrast the analysis of the intervals with low-amplitude movements reveals that the small-scale movements of both plates are well correlated, as if the bodies are tied to each other.

In case d1d2 after some wandering both plates are pressed against one wall, where they remain, occasionally breaking away from it for a short time. In case d1d3, the throws become stronger and the plates occasionally move from one wall to the other (remaining, as a rule, near the same wall), and the upper plate, unlike the lower one, does not press against the wall, remaining close to it. As the lower plate approaches the central plane, both plates are involved in intense, slightly correlated movements from one edge of the cavity to the other (cases d1d4 and d1d5). A strongly intermittent mode appears in case d1d6, in which very regular well correlated oscillations of both plates (just of the same kind as were observed in case d1d6 for larger plates, see Fig. 2) are replaced by quasi-periodic motions from the

FIG. 7. The movement of the centers of the plates of size $l = L/4$ at $\mathrm{Ra} = 3.7 \times 10^5$ for different cases, marked in each panel. The position of the lower plate is shown by blue dotted line, the position of the upper plate – by red solid line.

wall to the center and back of the upper plate, and small amplitude oscillations of the lower plate near the other wall. The latter behavior becomes stable in case d1d7 (last panel in Fig. 7). Finally, let us note, that despite evident differences in the plate dynamics for cases

d1d1, d1d4 and d1d5, the plate movements for all these cases are uncorrelated (the Pearson correlation is equal, respectively to -0.07, -0.2 and 0.04).

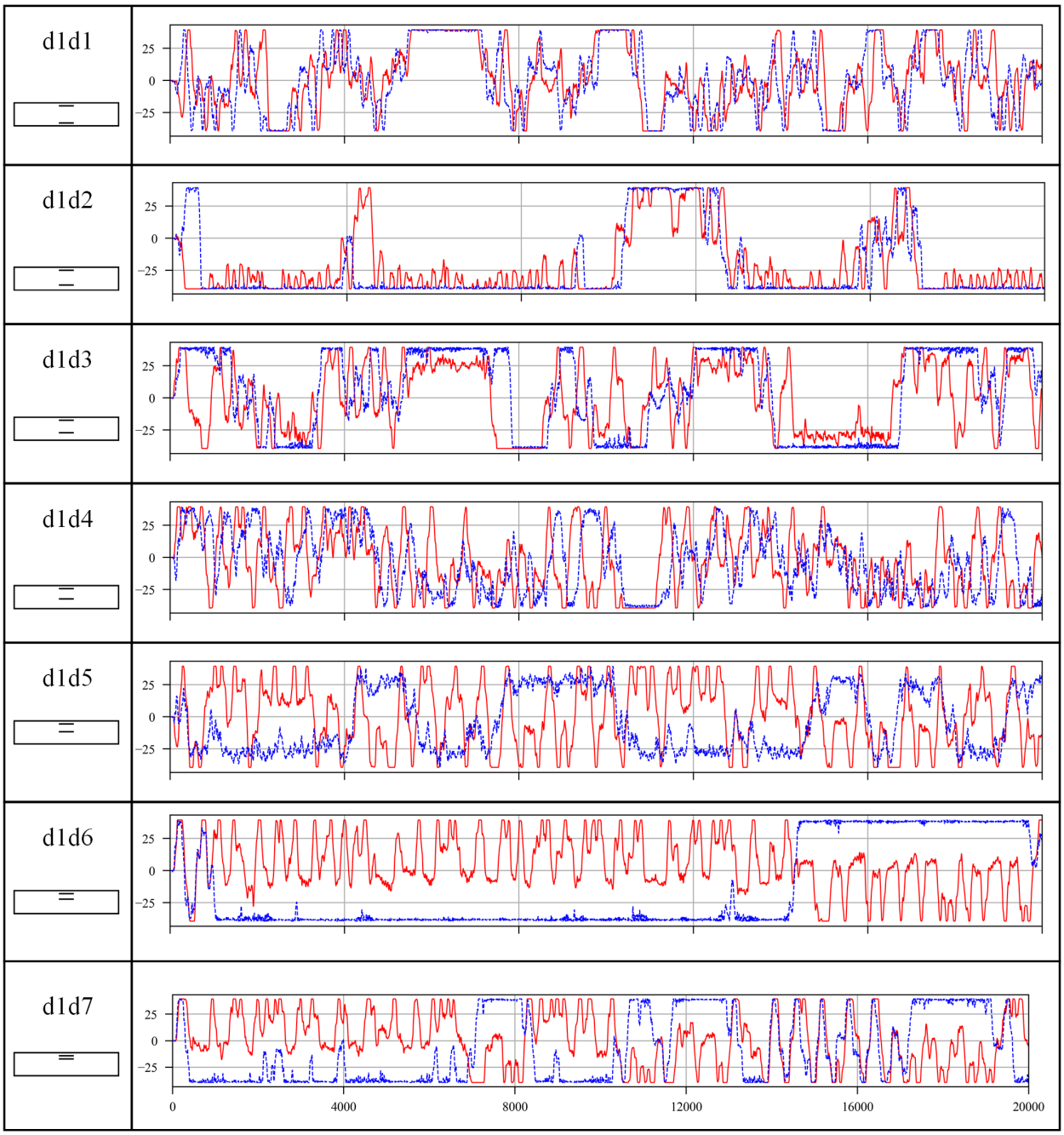

FIG. 8. The movement of the centers of the plates of size $l = L/8$ at $\mathrm{Ra} = 3.7 \times 10^5$ for different cases, marked in each panel. The position of the lower plate is shown by blue dotted line, the position of the upper plate – by red solid line.

Analyzing the dynamics of the smallest of the considered plates, having a size of $l = L/8$

(see Fig. 8), it can be concluded that their movements become less dependent on each other and the amplitude of high-frequency oscillations increases. At the same time, it is impossible not to notice the trend towards the relationship between the movement of the two plates. In cases d1d6 and d1d7, the behavior of the plates is generally similar to that of larger plates with $l = L/4$, but it is not periodic. They also prefer to locate near opposite walls with non-periodic motions in one half of the layer of the upper plate, and small amplitude oscillations of the lower plate. In contrast to this, if the plates are relatively far (cases d1d1, d1d2 and d1d3) they tends to follow one the other wandering from wall-to-wall, while performing intense small-scale independent fluctuations.

The tendency to correlated long-term dynamics is most pronounced in case d1d1 both for plates $l = L/4$ and $l = L/8$ and we analyse them in more detail. Note, that to improve the statistics we extend the duration of each run up to 20,000 seconds. Interestingly, when watching the movie of the small plate motion (see Supplementary materials), there is a deceptive feeling that the movement of the plates is chaotic and fully independent. At the same time, when looking at Fig. 8 it seems obvious that both trajectories follow each other, although they do not repeat each other in detail.

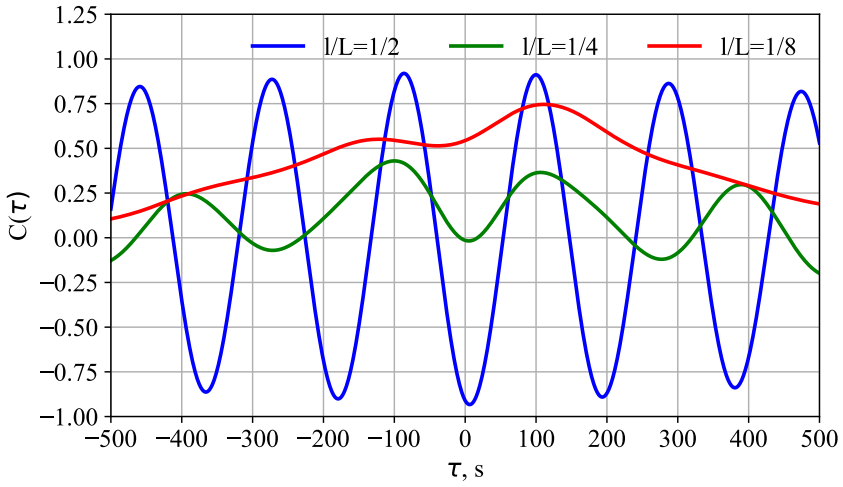

FIG. 9. The cross-correlation function of the positions of the centers of two plates moving near two heat exchangers (case d1d1) at Ra $= 3.7 \times 10^5$. The size of the plates is $l = L/2$ (blue line), $l = L/4$ (green line) and $l = L/8$ (red line).

The coherence of the movements of both plates is characterized by the cross-correlation function of the positions of their centers, shown in Fig. 9 for plates of different sizes in

case d1d1 (each plate is located at a distance of $H/10$ from the corresponding horizontal boundary) under the same Rayleigh number $\mathrm{Ra} = 3.7 \times 10^5$. For long plates, where $l = L/2$, a slightly damped cosine wave indicates nearly perfectly periodic motions of the plates in antiphase, $C(0) = -0.95$. At $l = L/4$, the one-time correlation disappears $C(0) \approx 0$, although local maxima of the order of $0.35 - 0.4$ remain on shifts of $\tau \approx \pm 100$s. At $l = L/8$, the correlation function becomes asymmetric relative to zero, showing a fairly significant correlation of $C \approx 0.75$ at $\tau = 100$c. The interpretation of the last two cross-correlation functions is difficult due to the rather complex structure of the analyzed movements.

A scale-by-scale cross-correlation analysis of two signals, which separates the correlation at different time-scales, can be done in term of wavelet analysis [22]. To do this, it is necessary to obtain a wavelet image of each signal (oscillograms of position of corresponding plate center)

$$w(\tau, t') = \tau^{-1/2} \int_{-\infty}^{\infty} x_i(t) \psi^* \left(\frac{t - t'}{\tau} \right) dt,$$
$$\psi(t) = e^{2\pi i t} e^{-t^2/2\sigma^2},$$

where x_i is the coordinate of the center of the corresponding plate ($i = 1.2$). A Morlet wavelet with the parameter $\sigma = 0.6$ was used, which provides a fairly good time resolution (short wave packet).

The wavelet spectrograms of the positions of the lower plates (they look similar for the upper ones) for plates of sizes $L/4$ and $L/8$ are shown in Fig. **??**. Integrating wavelet spectrograms along the horizontal coordinate (in time), one get the integral wavelet spectrum $M_i(\tau) = \int |w_i(\tau, t')|^2 dt'$, which is an analog of the spectral power density of fluctuations. Integral wavelet spectra are shown in Fig. 10(a). It can be seen that in the spectra for the $L/4$ plates there is a dominating frequency characterizing quasi-periodic fragments of the oscillogram. For $L/8$ plates, the low-frequency part of the spectra ($\tau > 200$ s) is almost flat, with an weak maximum at $\tau \approx 1200$ s, which corresponds to an average time of long stops of the plates near the sidewalls.

The wavelet cross-correlation function [22] is calculated for a pair of spectrograms characterizing the movements of the upper and lower plates in one numerical experiment

$$C_{12}(\tau) = \frac{\int w_1(\tau, t') w_2^*(\tau, t') dt'}{\left(M_1(\tau) M_2(\tau) \right)^{1/2}}.$$

This function characterizes the level of correlation of fluctuations in two signals at each given time scale τ.

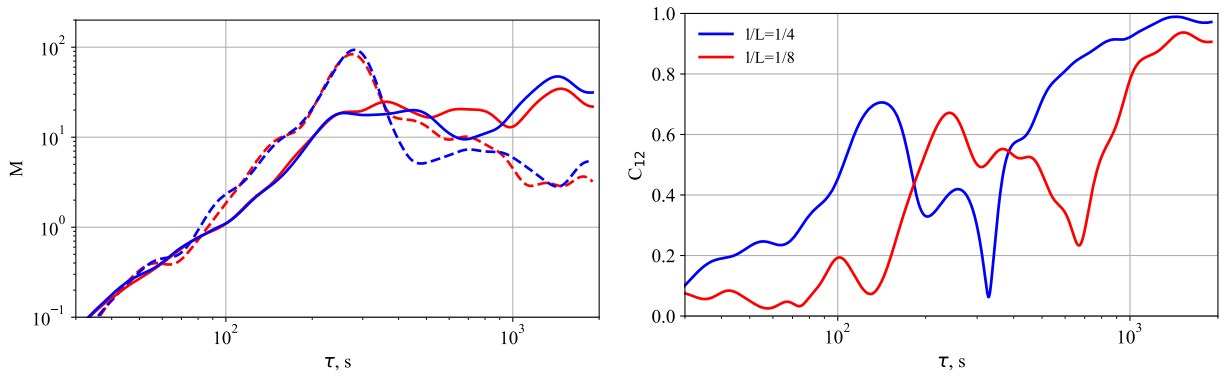

(a) (b)

FIG. 10. The integral wavelet spectrum (a) and the wavelet cross-correlation function (b) of the positions of the centers of the plates moving near two heat exchangers (case d1d1) at Ra = 3.7×10^5. The size of the plates is $l = L/4$ (dashed line) and $l = L/8$ (solid line). The blue line corresponds to the lower plate, the red line – to the upper plate.

The cross-correlation function $C_{12}(\tau)$, shown in Fig. 10,b confirms a high correlation of plate movements over long time scales. Small plates ($L/8$) give a correlation of 0.9 and higher at $\tau > 1000$s, and large plates ($l = L/4$) reach this correlation level at $\tau > 700$s. Both curves have a local maximum at shorter times, the first at $\tau \approx 240$s, and the second at $\tau \approx 120$s, with the height of the maxima approximately the same, $C_{12} \approx 0.65 - 0.7$. It would seem that these maxima are caused by fragments of quasi-periodic movements that are clearly visible on oscillograms, but their explanation is not so simple.

In Fig. 7 it can be seen that the oscillogram of plate movements (for case d1d1) includes sufficiently long intervals of quasi-stable periodic motions from one side wall to another, interspersed with intervals of random walks, in which, nevertheless, the oscillatory component of a small amplitude and approximately the same frequency exists. This is the frequency of the oscillations that corresponds to the maximum in the spectrum in Fig. 10. However, the peak in the spectrum occurs at periods of fluctuations of $\tau \approx 250$s, and the local maximum of the cross-correlation function (III C) falls at $\tau \approx 130$s, that is, approximately half as short. The analysis of the wavelet spectrogram (Fig. **??**,a) shows that $\tau \approx 130$s corresponds to structures that occur just in the intervals between full-scale oscillations of the plates from

wall to wall. Thus, fluctuations of relatively small amplitude, which accompany random plate walks, are correlated. The intervals of full-scale quasi-stable oscillations, which give a peak in the spectrum, are characterized by a random phase shift (either the upper plate follows the lower one, or vice versa), which leads to zero on average correlation.

There are no quasi-stable periodic oscillations from one edge to the other in the movements of the $L/8$ plates (Fig. 8), but a high-frequency component is present in most of the oscillogram, with the exception of fragments corresponding to the plate stopping at one of the side walls. For short periods, the small plates do not feel each other (at $\tau < 70$s, the curve tends to zero), while the plates ($l = L/4$) retain a weak correlation ($C \to 0.25$ at $\tau < 50$s). The local peak on the cross-correlation function at $\tau \approx 250$s (Fig. 10,b) is due to a series of bright spots visible at these time scales in the spectrogram (Fig. **??**,b), that is, not the presence of any long-term fluctuations, but rather a strong episode with an appropriate time scale. It is these episodes that turn out to be correlated.

D. Integral characteristics

The horizontal plate blocks the vertical fluid motion and heat flux, but the decrease of the values of the integral characteristics, such as Nusselt and Reynolds number strongly depends on the plate location [10, 11]. One can assume that introduction of the second plate would lead to the additional blocking of the vertical fluxes and decrease of Nu and Re.

The basic case is the pure Rayleigh-Bénard convection without plates (case d0d0). In order to reveal the influence of the plates on heat transport and flow intensity we presented in Fig. 11 normalized values of Nusselt number $\mathrm{Nu}/\mathrm{Nu}_0$ and Reynolds number $\mathrm{Re}/\mathrm{Re}_0$, where Nu_0 and Re_0 are the numbers, calculated for the convection in the same cell without plates. We include also in this figure the case with one plate (d1d0).

Fig. 11 shows that the heat transfer substantially depends on the mutual plate locations except the configuration with the smallest plates ($l = L/8$). In case d1d1, when both plates are located near horizontal boundaries and inside the thermal boundary layer, the heat exchange between the fluid and the warm (cold) boundary is significantly reduced. In this case, the large plates ($l = 3L/4$) that do not move, block almost 80% of the heat flux. Shifting one of the plates away from the horizontal boundary and, as a result from thermal boundary layer, increases heat transfer, reaching its maximum value in case d1d5. The

values of Nu for cases d1d4 – d1d6, when the plates can move independently, are close to those of a single plate floating in the fluid (d1d0). Further decreasing the gap between the plates (d1d7) leads to a noticeable decrease in the Nusselt number, despite different types of plate motion. It is a "sandwich" motion in the case of relatively large plates ($l = 3L/4$ and $l = L/2$), when they move as one thick plate. In the case of smaller plates ($l = L/4$), one of the plates oscillates near the wall, and the other plate periodically moves from the opposite wall to the center and back. The variation in Nu for the smallest plates ($l = L/8$) is minimal, as expected. Increase in Ra, which is considered only for the one plate size ($l = L/2$), gives qualitatively similar dependence of Nu on the plate locations (see open and closed squares in Fig. 11a).

The variation of the Reynolds number Re with the distance between plates is shown in Fig. 11b. The maximal values of Re for large plates ($l = 3L/4$ and $l = L/2$) are achieved for relatively small gaps between plates, when the plates moves together. Variation of Re for smaller plates are substantially weaker. Increasing of Ra does not change dependence of Re on the plate locations (for $l = L/2$). We can conclude that the introduction of a second plate in a layer reduces the heat flux and flow intensity. The maximal decrease occurs when both plates are close to horizontal boundaries. Shifting one of the plates from the thermal boundary layer increases both Nu and Re.

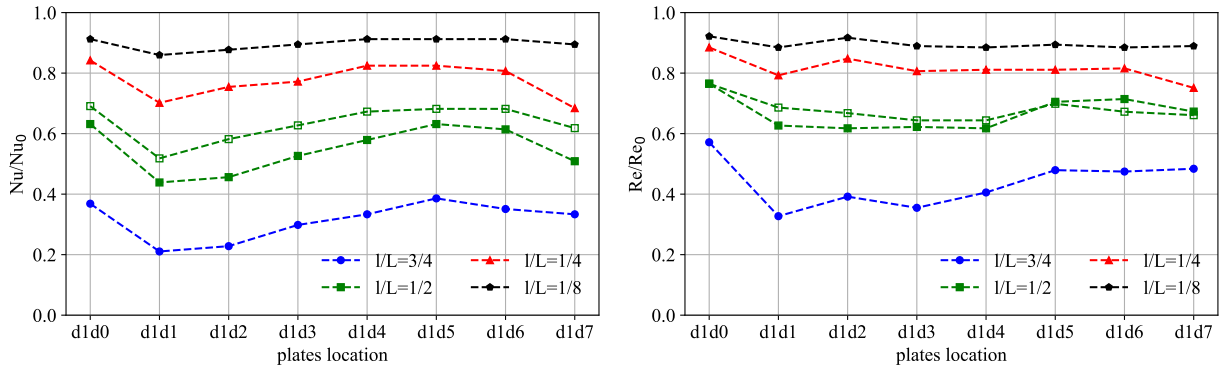

(a) (b)

FIG. 11. Normalized Nusselt number $\mathrm{Nu}/\mathrm{Nu}_0$ (a) and Reynolds number $\mathrm{Re}/\mathrm{Re}_0$ (b) for different cases and mutual plate locations, at $\mathrm{Ra} = 3.7 \times 10^5$ and $\mathrm{Ra} = 3.7 \times 10^6$ (only for $l = L/2$, shown by open squares), Nu_0 and Re_0 correspond to the case without plates (d0d0).

IV. CONCLUSION

An extended body, free floating nearby one of horizontal boundaries in a convective cell heated from below and cooled from above, with a suitable set of control parameters, provides the convective pendulum mode in which the body performs regular oscillatory movements from one side wall to the other. The mechanism of the convective pendulum is simple - the body, once at the side wall, blocks the heat flow near it, contributing to the appearance of a large-scale circulation in the cell, which draws the body to the opposite wall, where everything repeats. In this paper, we considered a cell with two bodies (plates) floating in a convective cell at different depths. Two convective pendulums in one cell are subject to a complex mutual influence determined by the geometry of the cavity, the size and the depth of immersion of the plates and the intensity of heating, which leads to a wide variety of observed modes. Some of them turned out to be completely unexpected, showing the presence of specific connections between bodies in convective systems.

The problem of two coupled convective pendulums is considered in the simplest two-dimensional formulation - we performed 2D numerical simulations of convective flow in an elongated rectangular cell with two plates having only one (horizontal) degree of freedom and located at different depths.

At moderate Rayleigh numbers ($\mathrm{Ra} \approx 5 \times 10^5$) the behavior of the extended plates with the sizes exceeding one half of the horizontal size of the convective cell is in general similar and strongly differs from that of the smaller plates. When the large plates are located near the horizontal boundaries the regime of the two-plate convective pendulum can be realized. If the lower plate shifted away from the bottom, the regularity of the movements of both plates is disrupted, including modes in which both plates stop in different positions and remain stationary until the end of the numerical simulation. When the gap between the plates decreases further they resume their movement. While the lower plate floats near the central plane, the plate movements are rather chaotic, but as the gap between plates decreases they become completely regular. Moreover, the movements of both plates become synchronized.

An increase in the heating intensity (Rayleigh number) leads to an acceleration of plate movement (an increase in the oscillation frequency) and the disappearance of the stagnation zone, in which irregular oscillatory movements occur. However, the type of mutual

movements of the plates generally remains the same.

An unexpected effect was found for the dynamics of two plates of relatively small size, (more precisely, with a size comparable to the thickness of the convective layer, but noticeably smaller than the horizontal cell size) which float in the vicinity of two heat exchangers. The modes with a pronounced intermittent character are identified, when intervals of quasi-periodic movements of both plates are replaced by low-amplitude oscillations against the background of random wandering throughout the cell. During full-amplitude oscillations, the plates move quasi-periodically but with a random phase shift. The very specific behavior was observed during random walks, in which the plates perform small-scale chaotic oscillations, without breaking away from each other, as if they were on a flexible bundle. For the smallest plates, whose size is significantly less than the depth of the layer, the quasi-periodic fragments of behavior do not occur, but, surprisingly, the "flexible bundle" continues to work. In this mode the plates tend to follow each other, despite stronger fluctuations, and if they locate at the sidewalls for a long time, it is always the same wall.

An increase in plate size reduces convective heat transfer and the intensity of flow motions (Nusselt and Reynolds numbers), however not proportionally to the plate sizes. For the fixed plate size the Nusselt number is minimal when the plates move in anti-phase near the thermal boundary layers. The shifting one of the plates from the boundary layer leads to an increase in the Nusselt number, and its maximum value is reached when both plates move synchronously in the same half of the fluid layer.

ACKNOWLEDGMENTS

The study was done under the RSF project 22-61-00098.

---

[1] G. Ahlers, S. Grossmann, and D. Lohse, Heat transfer and large scale dynamics in turbulent Rayleigh–Bénard convection, Reviews of modern physics **81**, 503 (2009).

[2] F. Chillà and J. Schumacher, New perspectives in turbulent Rayleigh–Bénard convection, The European Physical Journal E **35**, 58 (2012).

[3] O. Shishkina, Rayleigh–Bénard convection: The container shape matters, Physical Review Fluids **6**, 090502 (2021).

[4] J. Zhang and A. Libchaber, Periodic boundary motion in thermal turbulence, Physical Review Letters **84**, 4361 (2000).

[5] E. N. Popova and P. G. Frik, Large-scale flows in a turbulent convective layer with an immersed moving thermal insulator, Fluid Dynamics **38**, 862 (2003).

[6] J. Q. Zhong and J. Zhang, Modeling the dynamics of a free boundary on turbulent thermal convection, Phys. Rev. E **76**, 016307 (2007).

[7] Y. Mao, J. Q. Zhong, and J. Zhang, The dynamics of an insulating plate over a thermally convecting fluid and its implication for continent movement over convective mantle, Journal of Fluid Mechanics **868**, 286 (2019).

[8] Y. Mao, An insulating plate drifting over a thermally convecting fluid: the effect of plate size on plate motion, coupling modes and flow structure, Journal of Fluid Mechanics **916**, A18 (2021).

[9] W.-T. Wu, J. Zhang, and J.-Q. Zhong, Stochastic and deterministic dynamics of free boundaries atop turbulent convection, Physical Review Fluids **10**, 053504 (2025).

[10] P. Frick, S. Filimonov, A. Gavrilov, E. Popova, A. Sukhanovskii, and A. Vasiliev, Rayleigh–Bénard with immersed floating body, Journal of Fluid Mechanics **979**, A23 (2024).

[11] S. Filimonov, A. Gavrilov, K. Litvintsev, A. Vasiliev, A. Sukhanovskii, and P. Frick, Travelling of a reflecting immersed disk in a convective layer heated by incident radiation, Computational Continuum Mechanics **18**, 112–121 (2025).

[12] P. Frick, E. Popova, A. Sukhanovskii, and A. Vasiliev, A random 2d walk of a submerged free-floating disc in a convective layer, Physica D Nonlinear Phenomena **455**, 133882 (2023).

[13] P. Frick, S. Filimonov, A. Gavrilov, K. Litvintsev, A. Sukhanovskii, E. Popova, and A. Vasiliev, Dynamics of a submerged plate of different optical properties in a heated by radiation convective cell, Int. J. Heat Mass Transf. **241**, 126675 (2025).

[14] B. Liu and J. Zhang, Self-induced cyclic reorganization of free bodies through thermal convection, Physical review letters **100**, 244501 (2008).

[15] J. Lowman, S. King, and S. Trim, The influence of plate boundary motion on planform in viscously stratified mantle convection models, Journal of Geophysical Research: Solid Earth **116** (2011).

[16] S. Filimonov, A. Gavrilov, A. Dekterev, and K. Litvintsev, Mathematical modeling of the interaction of a thermal convective flow and a moving body, Computational Continuum Me-

chanics **16**, 89 (2023).

[17] S. Filimonov, A. Gavrilov, P. Frick, A. Sukhanovskii, and A. Vasiliev, 2D and 3D numerical simulations of a convective flow with a free-floating immersed body, Heat Transfer Research 10.1615/HeatTransRes.2024054471 (2024).

[18] R. Mittal and G. Iaccarino, Immersed boundary methods, Annu. Rev. Fluid Mech. **37**, 239 (2005).

[19] J. P. Van Doormaal and G. D. Raithby, Enhancements of the simple method for predicting incompressible fluid flows, Numerical heat transfer **7**, 147 (1984).

[20] C. M. Rhie and W.-L. Chow, Numerical study of the turbulent flow past an airfoil with trailing edge separation, AIAA journal **21**, 1525 (1983).

[21] F.-S. Lien and M. Leschziner, Upstream monotonic interpolation for scalar transport with application to complex turbulent flows, International Journal for Numerical Methods in Fluids **19**, 527 (1994).

[22] P. G. Frick, D. D. Sokoloff, and R. A. Stepanov, Wavelets for the space-time structure analysis of physical fields, Physics Uspekhi **65**, 62 (2022).